

MMFNet: A Multi-modality MRI Fusion Network for Segmentation of Nasopharyngeal Carcinoma

Huai Chen, Yuxiao Qi, Yong Yin, Tengxiang Li,
Guanzhong Gong*, Lisheng Wang*

Abstract—Segmentation of nasopharyngeal carcinoma (NPC) from Magnetic Resonance Images (MRI) is a crucial prerequisite for NPC radiotherapy. However, manually segmenting of NPC is time-consuming and labor-intensive. Additionally, single-modality MRI generally cannot provide enough information for its accurate delineation. Therefore, a multi-modality MRI fusion network (MMFNet) based on three modalities of MRI (T1, T2 and contrast-enhanced T1) is proposed to complete accurate segmentation of NPC. The backbone of MMFNet is designed as a multi-encoder-based network, consisting of several encoders to capture modality-specific features and one single decoder to fuse them and obtain high-level features for NPC segmentation. A fusion block is presented to effectively fuse features from multi-modality MRI. It firstly recalibrates low-level features captured from modality-specific encoders to highlight both informative features and regions of interest, then fuses weighted features by a residual fusion block to keep balance between fused ones and high-level features from decoder. Moreover, a training strategy named self-transfer, which utilizes pre-trained modality-specific encoders to initialize multi-encoder-based network, is proposed to make full mining of information from different modalities of MRI. The proposed method based on multi-modality MRI can effectively segment NPC and its advantages are validated by extensive experiments.

Index Terms—nasopharyngeal carcinoma, segmentation, multi-modality MRI, fusion block, self-transfer.

I. INTRODUCTION

NASOPHARYNGEAL carcinoma (NPC), which has an unknown and complicated etiology, is a kind of malignant tumor. The distinctive geographic distribution of NPC makes some regions such as Southeast Asia, South China, the Arctic and the Middle East/North Africa have extremely higher incidence than other regions [1]. Patients with early detection and diagnosis of NPC will have a greater 10-year survival rate with 98% for stage I and 60% for stage II, while the median survival of patients at advanced stage is only 3 years [2]. Therefore, timely and effective treatments play a crucial role in reducing the mortality of NPC. Radiotherapy, which highly depends on medical images such as the Magnetic

Resonance Images (MRI) to get accurate delineation of the gross tumor volume (GTV) to separate normal adjacent tissues from lesion regions to reduce radiation-associated toxicity [3], is the mainstay of treatment for NPC. However, clinicians need to manually mark the boundary of NPC slice by slice before developing radiotherapy plans currently, which is time-consuming and labor-intensive. Additionally, the quality of manual segmentation highly depends on the experience of clinicians, which influences treatment effect. Therefore, an automatic and accurate segmentation approach is urgently needed to alleviate the workload of clinicians and improve the efficacy of treatment presently.

Recently, according to the type of features used, methods of NPC segmentation can be divided into two categories, one is based on traditional handcrafted features, and the other one is based on deep features obtained from deep neural network (DNN). In traditional methods, besides relatively simple manual features of medical images, such as intensity [4], [5], texture [6] and shape [7], [8], some traditional knowledge-based methods such as support vector machine (SVM) [9], [10], semi-supervised fuzzy c-means [6], [11], dictionary learning [12] are also implemented to generate NPC boundary. Huang et al. [8] proposed a three-step NPC segmentation method in MRI. In this method, an adaptive algorithm and a distance regularized level set were applied to obtain the region of NPC and the contour, then a novel HMRF-EM framework based on the maximum entropy is presented to further refine segmentation results. Wang et al. [12] introduced a joint dictionary learning methods, which obtains simultaneously multiple dictionaries of CT, MRI and corresponding label, to achieve NPC segmentation.

Frameworks based on handcrafted features and traditional knowledge-based methods have been successfully implemented in the aforementioned papers to complete NPC segmentation in medical images. Nevertheless, the complex anatomical structure of NPC and the similarity of intensities between nearby tissues make it difficult to be accurately segmented only with the help of manual features. Meanwhile, the high diversity of shapes and sizes makes this task more challenging [8]. Therefore, inspired by the success of deep learning technology, some methods [13]–[15] based on DNN were proposed to get more accurate segmentation in recent years. Ma et al. [13] developed an image-patch-based convolutional neural network (CNN), integrating two CNN-based classification networks into a Siamese-like sub-network, to combine CT and T1-weighted (T1) images to complete NPC segmentation. Ma et al. [14] proposed a method combining

*Corresponding authors

This work has been submitted to the IEEE for possible publication. Copyright may be transferred without notice, after which this version may no longer be accessible.

H. Chen is with Institute of Image Processing and Pattern Recognition, Department of Automation, Shanghai Jiao Tong University, Shanghai, 200240, P. R. China.

*G. Gong is with Shandong Cancer Hospital Affiliated to Shandong University, Jinan, 250117, P.R. China.

*L. Wang is with Institute of Image Processing and Pattern Recognition, Department of Automation, Shanghai Jiao Tong University, Shanghai, 200240, P. R. China.

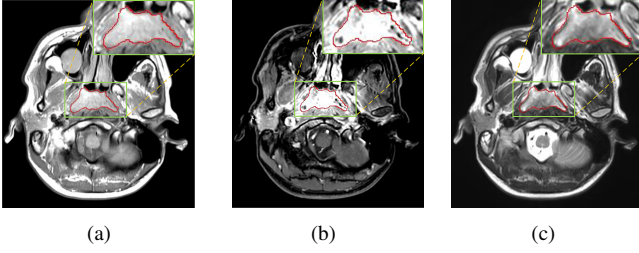


Fig. 1: Examples of slices from different MRI (T1, CET1 and T2), the contour of NPC is marked in red line. (a), (b) and (c) are slices from T1, CET1 and T2 respectively.

CNN and graph cut. According to this framework, the initial segmentation was firstly generated through integrating results obtained from three CNN-based networks focusing on axial, sagittal and coronal view. Then, a 3D graph-cut-based method was utilized to further refine it.

Previous deep-learning-based researches have established some excellent frameworks for NPC segmentation. Nevertheless, there remain the following deficiencies.

- (1) Although some DNN-based frameworks have been proposed recently to improve the performance of NPC segmentation [13]–[15], all of them are patch-based methods, which use a fixed-scale sliding window to crop image and determine the class of the central point. The performance of these frameworks highly depends on the scale of sliding window and is dramatically time-consuming due to severe computing redundancy. What's worse, all of above methods make predictions based on 2D slices of medical images, which ignores the vital role that 3D information plays in decision-making. Although Ma et al. [14] propose a method utilizing information of three-views to make decisions, this framework still fails to make full use of 3D information.
- (2) Currently, there is still no effort to fuse multi-modality MRI to develop an automatic segmentation system for NPC. For delineation of NPC, MRI is the preferred imaging modality for its superior soft tissue contrast [3], [16], [17]. Moreover, MRI of different modalities data have different visual characteristics and various responses to different tissues and anatomical structures. For example, T1-weighted (T1) MRI is suitable for detecting skull base involvement and fat planes, while contrast-enhanced T1-weighted (CET1) MRI is used to identify tumor extent [3]. Figure 1 shows some examples of NPC response in T1, CET1 and T2-weighted (T2) MRI. Meanwhile, according to researches of Popovtzer et al. [17], it should be a routine clinical practice to incorporate all kinds of MRI datasets in highly conformal radiation therapy to realize GTV delineation of NPC. What's more, using multi-modality MRI data to generate the boundary of brain tumors like gliomas and glioblastomas is a generally accepted practice [18]–[21].

In this paper, we try to improve NPC segmentation by fusing multi-modality MRI (T1, CET1, T2), and a multi-modality MRI fusion network (MMFNet) is developed. In the MMFNet,

the backbone, which is designed as a multi-encoder-based network and consists of several modality-specific encoders and one single decoder, can be used to well learn both low-level and high-level features used implicitly for NPC segmentation in each modality of MRI. The low-level features learned from multi-modality MRI will be recalibrated and fused by a fusion block that is specifically designed in the MMFNet for information fusion. The fusion block will firstly highlight those features that are highly relevant to NPC segmentation in each modality of MRI, and concentrate the attention on the regions of interest (ROIs). Then a residual fusion block is utilized to fuse re-weighted features and further refine the fused results to keep balance between them and high-level features. By decoder, the information from low-level and high-level features of multi-modality MRI can be effectively fused for the NPC segmentation. Additionally, a training strategy named self-transfer is used to effectively initialize encoders, which can stimulate different encoders to make full mining of modality-specific features. By the MMFNet, NPC can be well segmented with a high accuracy. We implement extensive experiments and comparisons with the related methods to demonstrates its effectiveness and advantages.

The main contributions of this paper can be summarized as followed:

- (1) This is the first multi-encoder framework that effectively segments NPC by fusing multiple modalities of MRI (T1, CET1, T2).
- (2) A novel fusion block is designed in the MMFNet, which can highlight features highly relevant to the NPC and put attention on the regions on interest. It facilitates to learn complementary features and cross-modal interdependencies from multi-modality MRI, and is helpful for the extraction of informative features for NPC segmentation.
- (3) By the multi-encoder single-decoder network and the fusion block, the fused features actually contain information from local regions, global regions and different modalities of MRI, which effectively improves NPC segmentation.
- (4) The training strategy named self-transfer can stimulate different encoders to make full mining of specific features from multi-modality MRI.

The remaining paper is organized as followed. In section II, related works will be reviewed. Section III will introduce our proposed framework. Experimental results and analysis will be reported in section IV. Then in section V we will set some ablation experiments to further discuss proposed method. Finally, a conclusion will be made in section VI.

II. RELATED WORK

A. Multi-modal fusion

In medical images, combining multi-modality images such as CT, T1 MRI, T2 MRI, etc. to realize multi-organ segmentation [22] and lesion segmentation [18], [19] is widely adopted due to distinct responses of different modalities datasets for different tissues. In general, there exist two major frameworks of multi-modality-based methods. The first one is single-encoder-based method [23], [24], which stacks multi-modality images channel-wise and feeds them into one single decoder.

The other one is multi-encoder-based method [18], [22], which uses multiple modality-specific encoders to extract feature maps at various levels and feeds them into one single decoder to fuse them. According to several researches [22], [25], methods based on multiple encoders have better capability to capture complementary and cross-modal interdependent features than single-encoder-based methods.

Although multi-encoder-based methods can combine information from multi-modality datasets to capture complementary and interdependent features, some individual features of specific modality can still be ignored. To address this problem, we present a training strategy named self-transfer to make full mining of individual features. And these features will be further fused to get interdependent cross-modality features. There also exist problems when we fuse features from different sources. The differences among low-level features from different modalities of MRI and the large imbalance in the channel numbers between low-level and high-level features can make network confused if we only simply combine them. Therefore, a fusion block is proposed to fuse low-level features and prepare fused ones for the fusion with high-level features. The fusion block can adaptively recalibrate low-level features from modality-specific encoders and fuse them into features with the same channel number of corresponding high-level features to keep balance between high-level and low-level features.

B. Attention mechanism

In human perception, the information gained from different sensory channels will be weighted by attention mechanism, namely, greater weights will be ascribed to sensory streams providing reliable information from the world [26]. Specially, in human visual attention mechanism, only a subset of sensory information will be selected by intermediate and higher visual processes to be further processed [27]. The idea of attention mechanism has been successfully implemented in several DNN-based frameworks for image classification [28]–[30], image understanding [31], target detection [30], etc..

For attention mechanism, channel attention modules and spatial attention modules are two major topics. Channel attention modules attempt to adaptively recalibrate channel-wise feature responses. SENet [29] is a typical representation for channel-attention-based framework, which proposes a block named *Squeeze-and-Excitation* (SE) block to modelling interdependencies between channels and generate a series of coefficients to highlight informative features. Compared to channel attention modules, spatial attention models emphasize the usage of concentrating on ROIs. Wang et al. [28] presented Residual Attention Network to utilize soft weight mask generated by a soft mask branch to decide where to be concentrated on. In addition to using one of these two modules separately, there also exist methods combining both of them. CBAM [30] is a lightweight architecture simultaneously employs both spatial and channel-wise attention to improve performance of DNN. In this method, both max-pooling outputs and average-pooling outputs are fed into a shared multi-layer perceptron (MLP) to obtain channel-wise attention. Meanwhile, similar

pooling outputs along channel axis are fed into a convolutional block to produce spatial attention.

In order to realize effective fusion of low-level features, we recalibrate low-level features from multiple encoders with the assistance of attention mechanism before fusing them to reduce confusion caused by differences among different features. We design a channel attention block and a spatial attention block to highlight informative features and ROIs. For the design of channel attention block, in order to provide more sufficient information for 3D MRI, besides max-values and average-values, standard deviations (stds) are also captured to make final channel-wise weights. Meanwhile, stds are also adopted to improve the performance of spatial channel block. Additionally, we respectively set three MLPs for these three kinds of features due to the huge differences among the distribution of average-values, max-values and stds.

III. METHODOLOGY

As illustrated in Figure 2, our framework is an end-to-end fully convolutional network, containing three encoders to take 3D-patch images from three modalities of MRI as inputs. The encoder network is a VGG-like [32] DNN, which stacks base block containing several convolution layers followed by max-pooling layers to get deeper features. And the decoder network uses deconvolutional layers to upsample feature maps, the final output is a feature map with the same size as input. Both low-level features and high-level features, which are relevant to NPC segmentation, can be obtained by the design of multiple encoders and one single decoder. In order to effectively fuse low-level features from multi-modality MRI and keep balance between high-level and low-level features, a fusion block is proposed to recalibrate and fuse multi-source low-level feature maps. For the training of network, we propose self-transfer to use pre-trained modality-specific encoders, which can capture individual modality-specific features from single modality MRI, as initial encoders of multi-modality model. The use of self-transfer can effectively improve the performance of encoders and make full mining of informative features from every modality of data.

A. Base encoder-decoder network

Inspired by U-net [33], our base encoder-decoder network can be seen as a U-net composed with 3D convolutional layers and 3D deconvolutional layers. Through stacking convolutional layers and max-pooling layers, encoder network can get larger receptive field, meanwhile, the spatial resolution becomes smaller. On the contrary, decoder network is composed with deconvolutional layers to upsample feature maps, thus, the spatial resolution of features can recover to original scale when high-level features go through it. As described in [34], higher layers capture high-level representations, which are necessary for recognize targets, and lower layers capture low-level representations such as texture, which play major roles in reducing the missing of tiny structures when we segment objects. Therefore, both content and style representations should be utilized to complete NPC segmentation. Thus, skip

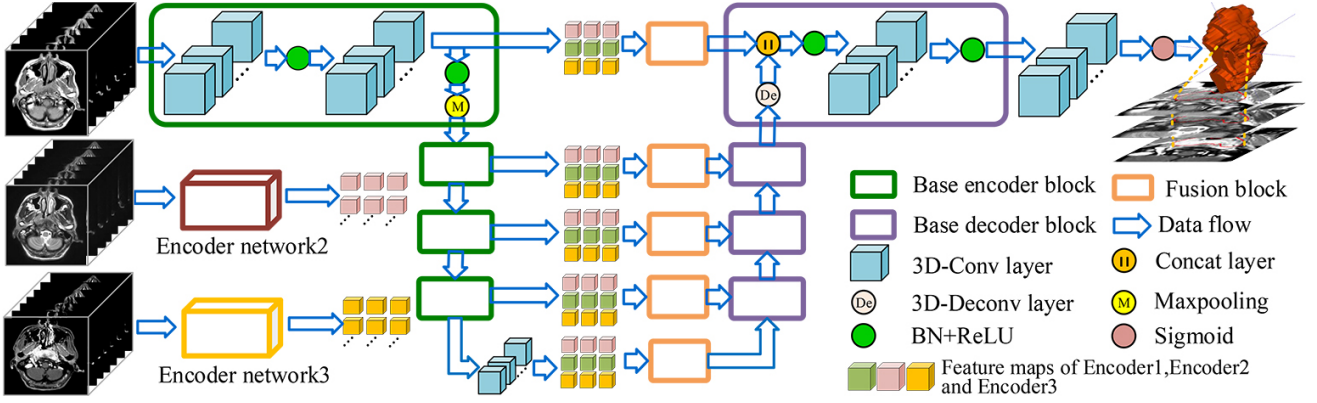


Fig. 2: An illustration of our proposed framework.

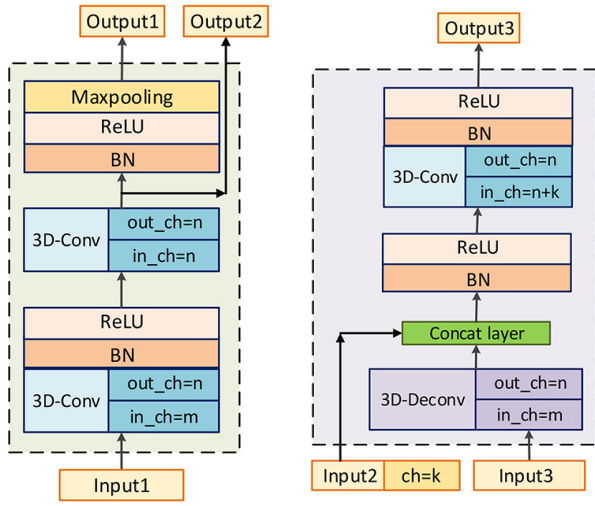


Fig. 3: An illustration of base encoder block and base decoder block. Left: base encoder block. Right: base decoder block. Input1, Input3: features from previous block. Input2: features produced by corresponding encoder block. Output1, Output3: features, which will be fed into next block. Output2: features, which will be fed into the corresponding decoder block through skip connection layer.

connection layers are adopted to combine low-level and high-level features. The architectures of base encoder block and decoder block are illustrated in Figure 3.

Base encoder network. Our encoder network is a VGG-like [32] network, and the base block is composed with two 3D convolutional layers. According to [35], the representation size should slightly decrease to avoid bottlenecks with enormous compression. Therefore, $3 \times 3 \times 3$ 3D convolutional layers and $2 \times 2 \times 2$ max-pooling layers are preferential choices to construct our network. And after convolution, a batch normalization layer and a ReLU layer are followed. There are two outputs produced by encoder block, one is for next encoder block, and the other one is for the corresponding decoder block to realize the combination of high-level and low-level features. There are totally four encoder blocks and the channel number of outputs (Out_ch) is 8, 16, 32 and

64 respectively. It is worth mentioning that there is one single convolutional layer after final encoder block to refine features downsampled by encoder block, and the number of its channels is 64.

Base decoder network. The purpose of decoder network is to map high-level features to target modality. A 3D deconvolutional layer is utilized to upsample feature maps, then, a concatenation layer combines these features with low-level features from encoders with the assistance of skip connection layers. After merging, a convolutional layer is adopted to fuse these feature maps. The numbers of output's channels for decoder blocks are 64, 32, 16 and 8 respectively.

Finally, the final decoder block is followed by a convolutional layer with sigmoid as activation to produce final segmentation results.

Loss function. Inspired by [36], which presents Dice coefficient to effectively solve imbalance between the numbers of voxels of foreground and background, we apply Dice loss as network's optimization objective. We denote ground truth as G and P is denoted as predict results. The definition of Dice loss is shown as:

$$Loss_{dice} = 1 - 2 \times \frac{\sum_{i=1}^N p_i g_i + \epsilon}{\sum_{i=1}^N p_i + \sum_{i=1}^N g_i + \epsilon} \quad (1)$$

$$p_i \in P \quad (2)$$

$$g_i \in G \quad (3)$$

Where ϵ is smoothness term to avoid the risk of division by 0, and we set $\epsilon = 1$ in our experiments.

B. Fusion block

The purpose of fusion block is to effectively recalibrate and fuse low-level features from different modalities of MRI before merging them with high-level features. It is a hard task to directly fuse low-level features from multiple MRI, which vary greatly from each other due to the varied responses to different tissues of multi-modality MRI. Therefore, the fusion block will firstly re-weighting features and highlight regions that are greatly relevant to NPC with the assistance of channel attention

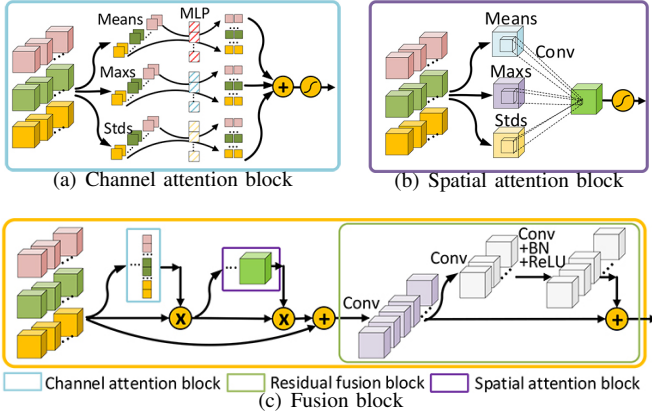


Fig. 4: The architecture of channel attention block, spatial attention block and fusion block.

and spatial attention block. After recalibrating low-level features, a residual fusion block is utilized to fuse them into ones with the same channel number of corresponding high-level features to keep balance between them. Specifically speaking, the fusion block is composed with a channel attention block, which focuses on 'what' are meaningful features, a spatial attention block, which focuses on where is an interesting part, and a residual fusion block, which is utilized to fuse weighted feature maps into ones with the same channel number as high-level features and refines them. The architectures of them are shown in Figure 4.

Given three intermediate feature maps from multiple encoders $F_1, F_2, F_3 \in R^{C \times D \times H \times W}$ as inputs. We firstly merge them on channel axis to obtain total original feature maps $F_{ori} \in R^{3C \times D \times H \times W}$. And we denote the final fused features as F_{fused} , the overall fusing process can be summarized as followed:

$$F_c = W_c(F_{ori}) \otimes F_{ori} \quad (4)$$

$$F_s = W_s(F_c) \otimes F_c \quad (5)$$

$$F_{fused} = Res(F_s + F_{ori}) \quad (6)$$

We denote \otimes as element-wise multiplication, which will automatically broadcast spatial attention weights (W_s) and channel attention weights (W_c) to fit input feature maps. Meanwhile, F_c and F_s are denoted as feature maps after being refined by channel attention block and spatial attention block respectively. F_{fused} is the final output, which is fused and refined by residual fusion block.

Channel attention block. The focus of channel attention block is to selectively emphasize feature maps, which are meaningful for final predictions. SENet [29] utilizes global average pooling to capture average-values of each feature map, and feeds them into a MLP to get weights for every channel. Compared to SENet, the channel attention block of CBAM [30] uses global max-pooling layers to get max-values of feature maps in addition to capturing average-values using global average-pooling layers. And both average-values and

max-values are fed into a shared MLP. Then, the output vectors are combined by add operation.

In this paper, in order to better represent the global features for 3D feature maps, we capture stds of every three-dimension features and combine them with average-values and max-values to produce weights for every channel feature. We denote obtained stds, average-values and max-values as $F_{std}, F_{avg}, F_{max} \in R^{3c \times 1 \times 1 \times 1}$. In terms of MLP, because there exist great gaps among the distribution of stds, average-values and max-values, we respectively set three MLPs for them. All of these MLPs are composed with one hidden layer setting hidden activation size as $R^{3c/r \times 1 \times 1 \times 1}$, where r is the reduction ratio and we set $r = 12$ in our experiments. And the final output channel weights W_c has $3c$ values for each channel feature. The formulation for W_c is shown as followed:

$$W_c(F_{ori}) = \sigma(MLP_{avg}(F_{avg}) + MLP_{max}(F_{max}) + MLP_{std}(F_{std})) \quad (7)$$

$$F_{avg} = AvgPool(F_{ori}) \quad (8)$$

$$F_{max} = MaxPool(F_{ori}) \quad (9)$$

$$F_{std} = StdPool(F_{ori}) = (AvgPool((F - AvgPool(F_{ori}))^2))^{1/2} \quad (10)$$

Where σ is the sigmoid activation to produce channel-wise weights varied from 0 to 1. Figure 4(a) shows the architecture of channel attention block.

Spatial attention block. The purpose of spatial attention block is to utilize feature maps after channel-wise refining to obtain 3D spatial attention map (W_s). On the basis of previous work of CBAM, we capture stds, average-values and max-values along the channel axis and concatenate them to generate three 3D feature blocks. And these features are fed into a $3 \times 3 \times 3$ 3D convolutional layer with sigmoid as activation to produce W_s . Through element-wise multiplication, informative regions will be effectively highlighted. The architecture of spatial attention block is shown in Figure 4(b), and the process can be summarized as followed:

$$W_s = \sigma(f^{3 \times 3 \times 3}([AvgPool(F_c); MaxPool(F_c); StdPool(F_c)])) \quad (11)$$

Where $f^{3 \times 3 \times 3}$ is denoted as one single convolutional layer with $3 \times 3 \times 3$ kernel size and the number of output's channels is 1.

Residual fusion block. After highlighting informative features and ROIs, a residual fusion block is constructed to fuse and refine low-level features. It is worth mentioning that the numbers of channels are $3c$ for $(F_{ori} + F_s)$, while the corresponding high-level features, which is prepared to combine with fused features, only has c channels. Therefore, in order to keep balance between low-level and high-level features, an $1 \times 1 \times 1$ convolutional layer with c channel outputs is utilized to fuse feature maps and reduce channel number firstly. Then, a residual block is adopted to refine feature maps. This block is composed with two convolutional layers, both of them have $1 \times 3 \times 3$ kernels and the first one is followed by a

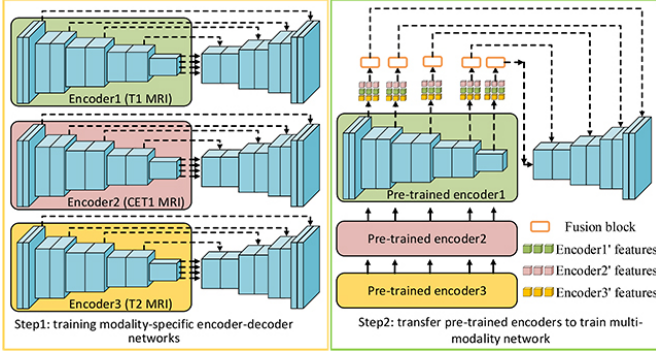


Fig. 5: An illustration of the self-transfer learning.

batch normalization layer and a ReLU layer. We can summary this process using following equations:

$$F_r = f^{1 \times 1 \times 1}(F_{ori} + F_s) \quad (12)$$

$$F_{fused} = F_r + f^{1 \times 3 \times 3}(f^{1 \times 3 \times 3}(F_r)) \quad (13)$$

Where F_r is feature maps after $1 \times 1 \times 1$ convolutional layer, and $f^{1 \times 3 \times 3}$ is denoted as $1 \times 3 \times 3$ convolutional layer followed by a batch normalization layer and a ReLU layer.

C. Self-transfer learning

Transfer learning [37] is a popular trick to improve performance of systems. Utilizing a powerful pre-trained network as features' extractor can bring dramatical improvements to new systems. Hence, using a network pre-trained in imagenet as an encoder for a segmentation network is a common operation in natural images [38], [39]. However, there is not a powerful enough 3D pre-trained model can be set as the initial features' extractor for various 3D medical images due to their complexity and various imaging technologies. Especially for multi-modality MRI, images of each modality have their own specific imaging styles, it's hard to obtain a feature extractor, which can be generalized to all of them. Additionally, by the design of multi-encoder single-decoder network, complementary information and cross-modal interdependencies can be extracted, while some individual features of specific modality may be ignored. To address these problems, we propose an initialization trick named self-transfer to effectively initialize encoders and make full mining of features of different modalities of MRI. According to experimental results, performance of multi-encoder-based models can obtain considerable improvements by using self-transfer.

Specifically speaking, a modality-specific model can effectively capture individual informative features from one single modality of data, while a multi-modality model aims to obtain interdependent and complementary information from multiple-modality datasets. As a result, some individual features of one single modality may be ignored in multi-modality model. Therefore, we propose self-transfer to fully mine modality-specific features. Figure 5 is the illustration of self-transfer. The first step is to train three modality-specific encoder-decoder models. Then, these pre-trained encoders will be used

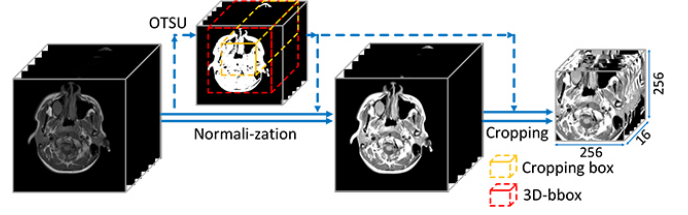


Fig. 6: An illustration of preprocessing.

as the initial encoders for multi-modality model. Compared to original encoders with random initialization, these encoders have greater power to make full mining of individual features from specific modality of MRI. Meanwhile, the fusion block and decoder can effectively fuse these features to obtain informative features for final predictions. We will set several experiments to demonstrate that self-transfer can enhance the segmentation systems in the following paper.

IV. EXPERIMENTS AND COMPARATION

A. Dataset and Preprocessing

Dataset. Three modalities of MRI of T1, CET1 and T2 of 149 patients are acquired at Shandong Cancer Hospital Affiliated to Shandong University. These patients are scanned with Philips Ingenia 3.0T MRI system. Both CET1 and T2 are aligned to T1. The spacings of X axis and Y axis are varied from $0.33mm$ to $0.69mm$, while the spacing of Z axis ranges from $3.5mm$ to $5.5mm$. So we resample the XY spacing to $0.5 \times 0.5mm^2$, and keep the spacing of Z fixed to avoid obtaining unreal images. The ground truth is created by an experienced radiologist and marked slice by slice.

Preprocessing. The preprocessing mainly contains intensity normalization and ROIs cropping. We utilize the intra-body intensity normalization proposed in [40], which effectively deals with the differences caused by imaging configurations and the influences of inconsistent body-to-background ratios. After normalization, according to the distribution histogram of normalized data, we clip (limit) values to reduce the complexity of data. Through statistical analysis for values in NPC regions, we set $[-2, 1]$, $[-3, 2]$ and $[-2, 3.5]$ for T1, T2 and CET1 respectively.

We use a sliding window to crop ROIs and feed them into network. Specifically speaking, we firstly use OTSU to get the 3D bounding box (3D-bbox) of original MRI and then we crop a $16 \times 256 \times 256$ region according to the central point of 3D-bbox. The sliding window slides on the Z axis and the sliding-step is 4. When feeding training samples, we perform on-the-fly data augmentation. Operations including random central offset from $(-4, -32, -32)$ to $(4, 32, 32)$, random vertical flipping and random rotation on the XY plane from -5° to 5° are applied. The illustration of preprocessing is shown in Figure 6.

B. Evaluation metrics

1) *Dice Similarity Coefficient (DSC)*: The dice similarity coefficient is designed to evaluate the overlap rate of predict

results and ground truth. DSC can be written as:

$$DSC(P, G) = \frac{2 \times |P \cap G|}{|P| + |G|} \quad (14)$$

DSC ranges from 0 to 1, and the better predict result will have a larger DSC.

2) *Average Precision (AP)*: It is the average precision score at different recall scores. We use different thresholding values to classify pixels into background or foreground and get several pairs of recall scores and precision scores. The definition of *AP* is shown as followed.

$$AP = \int_{recall=0}^{recall=1} precision \quad (15)$$

$$recall = \frac{TP}{TP + FN} \quad (16)$$

$$precision = \frac{TP}{TP + FP} \quad (17)$$

Where *TP* is the number of true positives, *FP* is the number of false positives and *FN* denotes the number of false negatives.

C. Experiments setting

The proposed MMFNet (MMFNet + multi-MLP + stdPool + self-transfer) is composed with three encoders for three modalities of MRI (T1, T2 and CET1), fusion blocks and one single decoder. There are three MLPs in channel attention block. And both channel attention block and spatial attention block contain std-pooling, max-pooling and average-pooling. In the training stage, we firstly train three modality-specific networks and then transfer the pre-trained encoders as the initial encoders for MMFNet. For the training of these modality-specific networks, we set Adam [41] as optimizer at a learning rate of 10^{-3} . While for the training of MMFNet, we firstly froze encoders' parameters in the first five epochs to warm up decoder with Adam at a learning rate of 10^{-3} . After decoder has been warmed up, we update both decoder and encoders of MMFNet with learning rate of 10^{-4} . The batch size for all MMFNet and modality-specific networks are 8. We set max epochs as 100 and networks will be updated 75 times each epoch.

MMFNet is evaluated in five-fold cross validation. And 25% of training data will be divided as validation data to choose best model and avoid overfitting. Meanwhile, we use early-stopping strategy to stop training if validation loss does not decrease over 10 epochs to reduce overfitting.

Our experiments are performed on a workstation platform with Intel(R) Xeon(R) CPU E5-2620 v4 @ 2.10GHz, 64GB RAM and 2x NVIDIA Titan Xp GPU with 12GB GPU memory. The code is implemented with pytorch 0.4.1 in Windows 10.

D. Comparative experiments

In this subsection, we set extensive comparative experiments to show the performance of MMFNet. These methods are described as followed:

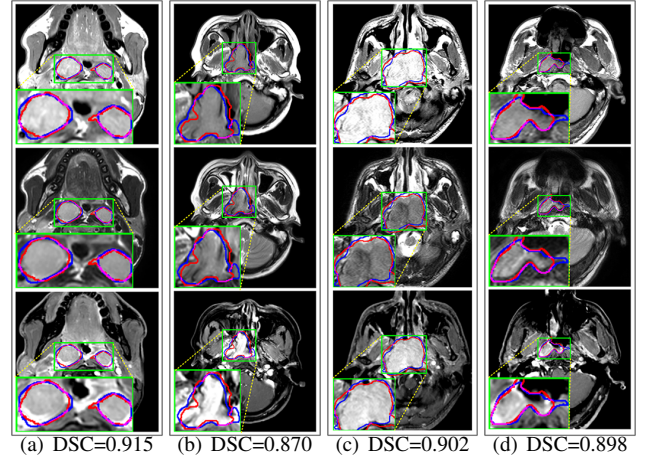


Fig. 7: Predicted results of proposed MMFNet in 2D images. There are corresponding T1, T2 and CET1 images from top to down. Boundaries created by radiologists are marked in red line, and the predicted boundaries are shown in blue line. The *DSC* value is the dice similarity coefficient of this single slice.

Patch-based CNN [14], [15], which utilizes a sliding window to capture patches of single-modality MRI to make decision whether the center point belongs to tumor. Multi-modality patch-based CNN [13] is a great method integrating multiple patch-based CNN into a Siamese-like sub-network to make predictions based on multi-modality medical images of NPC. The U-net [33], which is a novel end-to-end network for segmentation and is widely used in segmentation of medical images. The 3D U-net [42], which is the 3D vision of U-net. Single-encoder multi-modality network [23], [24], which stacks different modalities of MRI channel-wise as input for network. We concentrate three volumes of MRI as different input channel, the architectures of encoder and decoder are as described in III-A, while we set the channel number of encoder as three times of original encoder to keep the number of low-level features is the same as MMFNet. Multi-modality multi-encoder network [18], [22], which sets three modality-specific encoders to capture low-level features and a decoder to fuse low-level and high-level features. It's a degenerated MMFNet without fusion block and self-transfer.

E. Results

Comparison with ground truth. Some predicted results of MMFNet are shown in 2D images and 3D images in Figure 7 and Figure 8. As shown in these pictures, although the shape and size of NPC are varied from each other, MMFNet can still accurately determine the regions of NPC and obtain the accurate contours of tumors. Through analyzing 2D images in figure 7, MMFNet has a capacity to fuse multi-modality MRI to reduce the confusion brought by intensity' similarity between nearby tissues and NPC. The values of *DSC*, *AP* and *Loss_dice* of MMFNet are shown in Table I. MMFNet can reach the best results with $DSC = 0.7191$, $AP = 0.7721$ and $Loss_{dice} = 0.2907$.

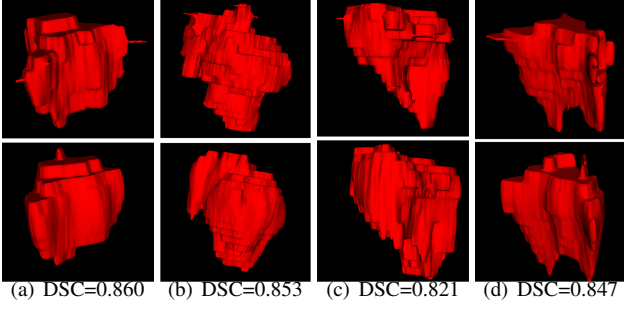


Fig. 8: Examples of 3D predicted results for MMFNet. The first row are ground truth, and the second row are masks predicted by MMFNet.

TABLE I: Comparison of NPC segmentation results using different methods.

Method	DSC	AP	$Loss_{dice}$
Patch-based CNN (T1)	0.5195	0.5320	0.4818
Patch-based CNN (T2)	0.4939	0.4984	0.5074
Patch-based CNN (CET1)	0.5693	0.5828	0.4314
Multi-modality patch-based CNN	0.6083	0.6307	0.3930
U-net (T1)	0.5895	0.6169	0.4119
U-net (T2)	0.5589	0.5777	0.4422
U-net (CET1)	0.6012	0.6142	0.3995
3D U-net (T1)	0.6817	0.7202	0.3361
3D U-net (T2)	0.6589	0.6920	0.3610
3D U-net (CET1)	0.6222	0.6456	0.3921
Single-encoder multi-modality network	0.6552	0.6954	0.3556
Multi-encoder multi-modality network	0.7005	0.7439	0.3141
MMFNet+multi-MLP+stdPool+self-transfer	0.7191	0.7721	0.2907

Comparison with related works. Table I reports the values of DSC , AP and $Loss_{dice}$ for different methods. Predicted masks of different methods are illustrated in Figure 9 and Figure 10, which respectively present results in 2D and 3D images. Through comprehensively analyzing these results, the proposed MMFNet actually have the following properties:

(i) It directly fuses 3D MRI images rather than 2D slices. Thus, it can effectively use meaningful information from neighboring slices of MRI to realize NPC segmentation. As shown in Table II, MMFNet can bring 11.08%, 14.14% and 0.1023 improvements in DSC , AP and $Loss_{dice}$ compared to the best method based on 2D images (Multi-modality patch-based CNN). And Figure 10 shows that 3D-based methods have less isolated regions (false positives) than 2D-based ones.

(ii) It segments NPC by fusing multi-modality MRIs with the multi-encoder network. Thus, it can learn complementary and interdependent features from different modalities of MRI for final decisions. Additionally, comparing with single-encoder-based networks, multi-encoder-based networks can effectively capture informative features from different modalities of MRI and fuse low-level features and high-level features. Compared with single-encoder-based network (Single-encoder multi-modality network), MMFNet improves the DSC , AP and $Loss_{dice}$ by 6.39%, 7.67% and 0.0649.

(iii) It uses a fusion block to fuse low-level features from different modalities of MRI and prepare these low-level fea-

tures for the fusion with high-level features. Thus, it can more effectively fuse information from various sources. It also uses the self-transfer skill to initialize the network. Hereby, it can stimulate different encoders to make full mining of meaningful features from modality-specific MRI. And it finally improve base multi-encoder multi-modality network by 1.86%, 2.82% and 0.0234 in DSC , AP and $Loss_{dice}$.

V. DISCUSSION

In this subsection, we set extensive ablation experiments to show the effectiveness of our proposed fusion block and self-transfer. The baseline is Multi-encoder based network.

The design for fusion block. The fusion block of base MMFNet is composed with 3D CBAM and residual fusion block, which utilizes a shared MLP in channel attention module and uses both max-pooling outputs and average-pooling outputs to obtain channel attention weights and spatial attention weights. Next, we modify single shared MLP into multiple MLPs for different global features. After that, we set several experiments to search best choice for the addition of std-pooling outputs.

According to results shown in Table II, the best design for fusion block is the one with multiple MLPs in channel attention block and with std-pooling in both channel attention and spatial attention blocks. The utilization of std-pooling outputs can provide more sufficient global information of 3D images, and the setting of multiple MLPs is suitable to deal with multiple features (outputs of std-pooling, max-pooling and average-pooling) with varied distributions.

The contribution of self-transfer. After setting several experiments to find the best design of fusion block, we implement self-transfer to these models to investigate its efficacies. We firstly train three modality-specific encoder-decoder network. Then, these pre-trained encoders aforementioned will be the initial features' extractors for several multi-modality networks with different fusion blocks.

Results in Table II show that the utilization of self-transfer can stimulate encoders to capture more meaningful features for NPC segmentation from MRI. All methods with self-transfer implemented in this paper can have better performances in evaluate metrics compared to corresponding methods without it. Therefore, self-transfer is a great strategy for multi-encoder-based network to realize NPC segmentation based on multi-modality MRI.

The choice of MRI. After demonstrating the effectiveness of MMFNet, we set several additional experiments to find the best combination of multi-modality MRI. We set three MMFNets with two encoders to show the results of methods based on only two modalities of MRI.

As shown in Table II, we come to the conclusion that fuse all modalities of MRI (T1, T2 and CET1) can obtain the best results. Various modalities of MRI have varied responses for different tissues. Combining all MRI to get complementary and interdependent information is meaningful for NPC segmentation.

It's worth mentioning that our proposed network is extremely time-friendly compared to manually marking by radiologists. Specifically speaking, our proposed method only

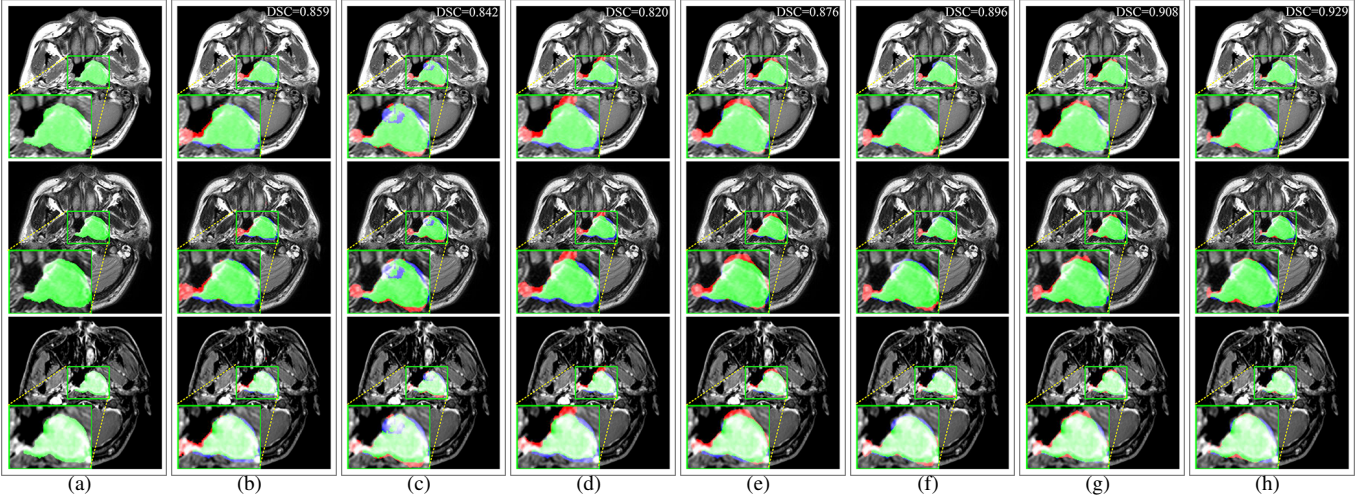


Fig. 9: Predicted results in one single slice image, there are corresponding T1, T2 and CET1 images from top to down. Green regions denote TP points, red and blue regions denote FP and FN point. (a) Ground truth. (b) Patch-based CNN (CET1). (c) Multi-modality patch-based CNN. (d) U-net (CET1). (e) 3D U-net (CET1). (f) Single-encoder multi-modality network. (g) Multi-encoder multi-modality network. (h) MMFNet + multi-MLP + stdPool + self-transfer.

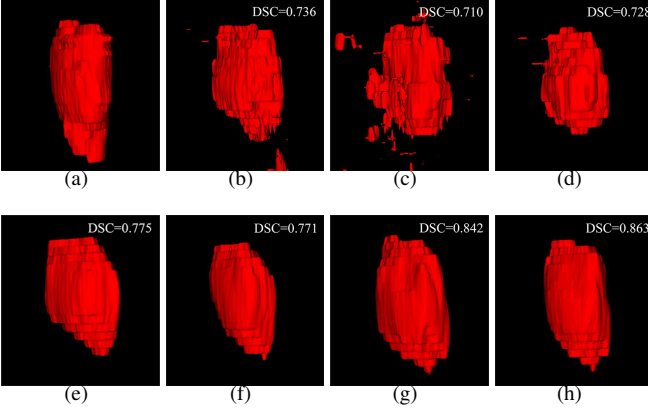


Fig. 10: Examples of 3D predicted results for different methods. (a) Ground truth. (b) Patch-based CNN (CET1). (c) Multi-modality patch-based CNN. (d) U-net (CET1). (e) 3D U-net (CET1). (f) Single-encoder multi-modality network. (g) Multi-encoder multi-modality network. (h) MMFNet + multi-MLP + stdPool + self-transfer.

needs about 9s to realize NPC delineation of a patient, while an experienced radiologist needs 10 to 20 minutes to complete it.

VI. CONCLUSION

In this paper, we propose a novel multi-modality MRI fusion network (MMFNet) to segment nasopharyngeal carcinoma (NPC) based on three MRI modalities (T1, T2 and contrast-enhanced T1). For this purpose, the backbone of the MMFNet is designed as a multi-encoder-based network, which can well learn both low-level and high-level features used implicitly for NPC segmentation in each modality of MRI. A fusion block is used in the MMFNet to effectively fuse low-level features from multi-modality MRI, whose design is inspired by attention mechanism of the human vision system and thus

TABLE II: NPC segmentation results of ablation experiments.

Method	DSC	AP	$Loss_{dice}$
Multi-encoder multi-modality network (baseline)	0.7005	0.7439	0.3141
Base MMFNet	0.7007	0.7494	0.3129
MMFNet+multi-MLP	0.7083	0.7508	0.3046
MMFNet+multi-MLP+stdPool (channel-attention)	0.7095	0.7602	0.3015
MMFNet+multi-MLP+stdPool (spatial-attention)	0.7010	0.7482	0.3123
MMFNet+multi-MLP+stdPool	0.7189	0.7648	0.2938
Base MMFNet+self-transfer	0.7095	0.7589	0.3018
MMFNet+multi-MLP+self-transfer	0.7128	0.7659	0.2971
MMFNet+multi-MLP+stdPool+self-transfer	0.7191	0.7721	0.2907
MMFNet+multi-MLP+stdPool+self-transfer(T1&T2)	0.7098	0.7598	0.3026
MMFNet+multi-MLP+stdPool+self-transfer(T1&CET1)	0.7034	0.7542	0.3079
MMFNet+multi-MLP+stdPool+self-transfer(T2&CET1)	0.6943	0.7372	0.3189

it can well highlight informative features and ROIs. The fusion block also plays a major role in keeping balance between low-level and high-level features. A training strategy named self-transfer is proposed to effectively initialize features extractors of MMFNet. Experiments show that, the MMFNet can well segment NPC with a high accuracy. Particularly, comparing with the existing related works, such as U-net, patch-based CNN and 3D U-net, MMFNet shows a big advantages in NPC segmentation.

Acknowledgment This work was supported in part by NSFC of China (61375020, 61572317), Shanghai Intelligent Medicine Project (2018ZHYL0217), and SJTU Translational Medicine Cross Research Fund (ZH2018QNA05).

REFERENCES

- [1] Mazin Abed Mohammed, Mohd Khanapi Abd Ghani, Raed Ibraheem Hamed, and Dheyaa Ahmed Ibrahim, "Review on nasopharyngeal carcinoma: Concepts, methods of analysis, segmentation, classification, prediction and impact: A review of the research literature," *Journal of Computational Science*, vol. 21, pp. 283–298, 2017.
- [2] Lei Wu, Churong Li, and Li Pan, "Nasopharyngeal carcinoma: A review of current updates," *Experimental and therapeutic medicine*, vol. 15, no. 4, pp. 3687–3692, 2018.

- [3] Ahmed Abdel Khalek Abdel Razek and Ann King, "Mri and ct of nasopharyngeal carcinoma," *American Journal of Roentgenology*, vol. 198, no. 1, pp. 11–18, 2012.
- [4] Chanon Tatanun, Panrasee Ritthipravat, Thongchai Bhongmakapat, and Lojana Tuntiyatorn, "Automatic segmentation of nasopharyngeal carcinoma from ct images: region growing based technique," in *Signal Processing Systems (ICSPS), 2010 2nd International Conference on*. IEEE, 2010, vol. 2, pp. V2–537.
- [5] Weerayuth Chanapai, Thongchai Bhongmakapat, Lojana Tuntiyatorn, and Panrasee Ritthipravat, "Nasopharyngeal carcinoma segmentation using a region growing technique," *International journal of computer assisted radiology and surgery*, vol. 7, no. 3, pp. 413–422, 2012.
- [6] Jiayin Zhou, Tuan-Kay Lim, Vincent Chong, and Jing Huang, "A texture combined multispectral magnetic resonance imaging segmentation for nasopharyngeal carcinoma," *Optical review*, vol. 10, no. 5, pp. 405–410, 2003.
- [7] Isabelle Fitton, SAP Cornelissen, Joop C Duppen, RJHM Steenbakkers, STH Peeters, FJP Hoebbers, Johannes HAM Kaanders, PJCM Nowak, Coen RN Rasch, and Marcel van Herk, "Semi-automatic delineation using weighted ct-mri registered images for radiotherapy of nasopharyngeal cancer," *Medical physics*, vol. 38, no. 8, pp. 4662–4666, 2011.
- [8] Kai-Wei Huang, Zhe-Yi Zhao, Qian Gong, Juan Zha, Liu Chen, and Ran Yang, "Nasopharyngeal carcinoma segmentation via hmrf-em with maximum entropy," in *Engineering in Medicine and Biology Society (EMBC), 2015 37th Annual International Conference of the IEEE*. IEEE, 2015, pp. 2968–2972.
- [9] Jiayin Zhou, Qi Tian, Vincent Chong, Wei Xiong, Weimin Huang, and Zhimin Wang, "Segmentation of skull base tumors from mri using a hybrid support vector machine-based method," in *International Workshop on Machine Learning in Medical Imaging*. Springer, 2011, pp. 134–141.
- [10] Wei Huang, Kap Luk Chan, and Jiayin Zhou, "Region-based nasopharyngeal carcinoma lesion segmentation from mri using clustering-and classification-based methods with learning," *Journal of digital imaging*, vol. 26, no. 3, pp. 472–482, 2013.
- [11] Jiayin Zhou, Vincent Chong, Tuan-Kay Lim, and J Houng, "Mri tumor segmentation for nasopharyngeal carcinoma using knowledge-based fuzzy clustering," *International journal of information technology*, vol. 8, no. 2, 2002.
- [12] Yan Wang, Biting Yu, Lei Wang, Chen Zu, Yong Luo, Xi Wu, Zhipeng Yang, Jiliu Zhou, and Luping Zhou, "Tumor segmentation via multi-modality joint dictionary learning," in *Biomedical Imaging (ISBI 2018), 2018 IEEE 15th International Symposium on*. IEEE, 2018, pp. 1336–1339.
- [13] Zongqing Ma, Xi Wu, Shanhui Sun, Chaoyang Xia, Zhipeng Yang, Shuo Li, and Jiliu Zhou, "A discriminative learning based approach for automated nasopharyngeal carcinoma segmentation leveraging multi-modality similarity metric learning," in *Biomedical Imaging (ISBI 2018), 2018 IEEE 15th International Symposium on*. IEEE, 2018, pp. 813–816.
- [14] Zongqing Ma, Xi Wu, Qi Song, Yong Luo, Yan Wang, and Jiliu Zhou, "Automated nasopharyngeal carcinoma segmentation in magnetic resonance images by combination of convolutional neural networks and graph cut," *Experimental and therapeutic medicine*, vol. 16, no. 3, pp. 2511–2521, 2018.
- [15] Yan Wang, Chen Zu, Guangliang Hu, Yong Luo, Zongqing Ma, Kun He, Xi Wu, and Jiliu Zhou, "Automatic tumor segmentation with deep convolutional neural networks for radiotherapy applications," *Neural Processing Letters*, pp. 1–12, 2018.
- [16] Julian Goh and Keith Lim, "Imaging of nasopharyngeal carcinoma," *Ann Acad Med Singapore*, vol. 38, no. 9, pp. 809–16, 2009.
- [17] Aron Popovtzer, Mohannad Ibrahim, Daniel Tatro, Felix Y Feng, Randall K Ten Haken, and Avraham Eisbruch, "Mri to delineate the gross tumor volume of nasopharyngeal cancers: which sequences and planes should be used?," *Radiology and oncology*, vol. 48, no. 3, pp. 323–330, 2014.
- [18] Kuan-Lun Tseng, Yen-Liang Lin, Winston Hsu, and Chung-Yang Huang, "Joint sequence learning and cross-modality convolution for 3d biomedical segmentation," in *Computer Vision and Pattern Recognition (CVPR), 2017 IEEE Conference on*. IEEE, 2017, pp. 3739–3746.
- [19] Chao Ma, Gongning Luo, and Kuanquan Wang, "Concatenated and connected random forests with multiscale patch driven active contour model for automated brain tumor segmentation of mr images," *IEEE Transactions on Medical Imaging*, 2018.
- [20] Hongmin Cai, Ragini Verma, Yangming Ou, Seung-koo Lee, Elias R Melhem, and Christos Davatzikos, "Probabilistic segmentation of brain tumors based on multi-modality magnetic resonance images," in *Biomedical Imaging: From Nano to Macro, 2007. ISBI 2007. 4th IEEE International Symposium on*. IEEE, 2007, pp. 600–603.
- [21] Bjoern H Menze, Andras Jakab, Stefan Bauer, Jayashree Kalpathy-Cramer, Keyvan Farahani, Justin Kirby, Yuliya Burren, Nicole Porz, Johannes Slotboom, Roland Wiest, et al., "The multimodal brain tumor image segmentation benchmark (brats)," *IEEE transactions on medical imaging*, vol. 34, no. 10, pp. 1993, 2015.
- [22] Vanya V Valindria, Nick Pawlowski, Martin Rajchl, Ioannis Lavdas, Eric O Aboagye, Andrea G Rockall, Daniel Rueckert, and Ben Glocker, "Multi-modal learning from unpaired images: Application to multi-organ segmentation in ct and mri," in *Applications of Computer Vision (WACV), 2018 IEEE Winter Conference on*. IEEE, 2018, pp. 547–556.
- [23] Mohammad Havaei, Axel Davy, David Warde-Farley, Antoine Biard, Aaron Courville, Yoshua Bengio, Chris Pal, Pierre-Marc Jodoin, and Hugo Larochelle, "Brain tumor segmentation with deep neural networks," *Medical image analysis*, vol. 35, pp. 18–31, 2017.
- [24] Konstantinos Kamnitsas, Christian Ledig, Virginia FJ Newcombe, Joanna P Simpson, Andrew D Kane, David K Menon, Daniel Rueckert, and Ben Glocker, "Efficient multi-scale 3d cnn with fully connected crf for accurate brain lesion segmentation," *Medical image analysis*, vol. 36, pp. 61–78, 2017.
- [25] Abhinav Valada, Gabriel L Oliveira, Thomas Brox, and Wolfram Burgard, "Deep multispectral semantic scene understanding of forested environments using multimodal fusion," in *International Symposium on Experimental Robotics*. Springer, 2016, pp. 465–477.
- [26] Harriet Feldman and Karl Friston, "Attention, uncertainty, and free-energy," *Frontiers in human neuroscience*, vol. 4, pp. 215, 2010.
- [27] Laurent Itti, Christof Koch, and Ernst Niebur, "A model of saliency-based visual attention for rapid scene analysis," *IEEE Transactions on pattern analysis and machine intelligence*, vol. 20, no. 11, pp. 1254–1259, 1998.
- [28] Fei Wang, Mengqing Jiang, Chen Qian, Shuo Yang, Cheng Li, Honggang Zhang, Xiaogang Wang, and Xiaoou Tang, "Residual attention network for image classification," in *Proceedings of the IEEE Conference on Computer Vision and Pattern Recognition*, 2017, pp. 3156–3164.
- [29] Jie Hu, Li Shen, and Gang Sun, "Squeeze-and-excitation networks," *arXiv preprint arXiv:1709.01507*, vol. 7, 2017.
- [30] Sanghyun Woo, Jongchan Park, Joon-Young Lee, and In So Kweon, "Cbam: Convolutional block attention module," in *Proceedings of the European Conference on Computer Vision (ECCV)*, 2018, pp. 3–19.
- [31] Long Chen, Hanwang Zhang, Jun Xiao, Liqiang Nie, Jian Shao, Wei Liu, and Tat-Seng Chua, "Sca-cnn: Spatial and channel-wise attention in convolutional networks for image captioning," in *2017 IEEE Conference on Computer Vision and Pattern Recognition (CVPR)*. IEEE, 2017, pp. 6298–6306.
- [32] Karen Simonyan and Andrew Zisserman, "Very deep convolutional networks for large-scale image recognition," *arXiv preprint arXiv:1409.1556*, 2014.
- [33] Olaf Ronneberger, Philipp Fischer, and Thomas Brox, "U-net: Convolutional networks for biomedical image segmentation," in *International Conference on Medical image computing and computer-assisted intervention*. Springer, 2015, pp. 234–241.
- [34] Leon A Gatys, Alexander S Ecker, and Matthias Bethge, "Image style transfer using convolutional neural networks," in *Proceedings of the IEEE Conference on Computer Vision and Pattern Recognition*, 2016, pp. 2414–2423.
- [35] Christian Szegedy, Vincent Vanhoucke, Sergey Ioffe, Jon Shlens, and Zbigniew Wojna, "Rethinking the inception architecture for computer vision," in *Proceedings of the IEEE conference on computer vision and pattern recognition*, 2016, pp. 2818–2826.
- [36] Fausto Milletari, Nassir Navab, and Seyed-Ahmad Ahmadi, "V-net: Fully convolutional neural networks for volumetric medical image segmentation," in *3D Vision (3DV), 2016 Fourth International Conference on*. IEEE, 2016, pp. 565–571.
- [37] Jason Yosinski, Jeff Clune, Yoshua Bengio, and Hod Lipson, "How transferable are features in deep neural networks?," in *Advances in neural information processing systems*, 2014, pp. 3320–3328.
- [38] Moke Yang, Kun Yu, Chi Zhang, Zhiwei Li, and Kuiyuan Yang, "Denseaspp for semantic segmentation in street scenes," in *Proceedings of the IEEE Conference on Computer Vision and Pattern Recognition*, 2018, pp. 3684–3692.
- [39] Hengshuang Zhao, Jianping Shi, Xiaojuan Qi, Xiaogang Wang, and Jiaya Jia, "Pyramid scene parsing network," in *IEEE Conf. on Computer Vision and Pattern Recognition (CVPR)*, 2017, pp. 2881–2890.
- [40] Yi-Jie Huang, Qi Dou, Zi-Xian Wang, Li-Zhi Liu, Ying Jin, Chao-Feng Li, Lisheng Wang, Hao Chen, and Rui-Hua Xu, "3d roi-aware u-net for

accurate and efficient colorectal tumor segmentation,” *arXiv preprint arXiv:1806.10342*, 2018.

- [41] Diederik P Kingma and Jimmy Ba, “Adam: A method for stochastic optimization,” *arXiv preprint arXiv:1412.6980*, 2014.
- [42] Özgün Çiçek, Ahmed Abdulkadir, Soeren S Lienkamp, Thomas Brox, and Olaf Ronneberger, “3d u-net: learning dense volumetric segmentation from sparse annotation,” in *International Conference on Medical Image Computing and Computer-Assisted Intervention*. Springer, 2016, pp. 424–432.